Computational Materials Science 245 (2024) 113294

Contents lists available at ScienceDirect

Computational Materials Science

journal homepage: www.elsevier.com/locate/commatsci

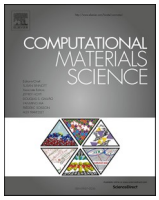

Full Length Article

Computational insights into the structural, thermodynamic and transport properties of CaF_2-MgF_2 binary fluoride system at high temperatures

Yifan Zhang [a], Rajni Chahal [b,1], M. Mustafa Azeem [a], Stephen Lam [b], Karl Ludwig [c], Uday Pal [c], Michael C. Gao [d], Adam Powell [a], Yu Zhong [a,*]

[a] Department of Mechanical & Materials Engineering, Worcester Polytechnic Institute, USA
[b] Department of Chemical Engineering, University of Massachusetts Lowell, USA
[c] Division of Materials Science & Engineering, Boston University, USA
[d] National Energy Technology Laboratory, USA

ARTICLE INFO

Keywords:
CaF_2-MgF_2 molten salt
ab initio molecular dynamics
Neural networks interatomic potentials
Radial distribution function
Angular distribution function
Matlantis

ABSTRACT

The structural, thermodynamic and transport properties of the CaF_2-MgF_2 molten salt system were investigated with ab initio molecular dynamics (AIMD), system-specific neural network interatomic potentials (NNIPs) and universal PreFerred Potentials (PFP). We trained an NNIP model using AIMD data as input and used this potential to efficiently simulate the interactions within a large supercell in a temperature range of 1273–1773 K. The Large-scale Atomic/Molecular Massively Parallel Simulator (LAMMPS) code was employed to validate our trained NNIP model. The Matlantis software with universal PFP is also presented to prove its feasibility for MD calculations and can be considered as a useful alternative simulation tool for higher-order systems where existing potentials are not readily available. We calculated structural and thermodynamic properties including radial distribution function (RDF), angular distribution function (ADF), specific heat capacity, ionic self-diffusivity, and viscosity. Our results indicate that the system exhibited a high degree of structural disorder, with the Ca, Mg, and F ions forming a liquid solution. Using PFP, the positions of the first peak in RDFs for Ca-F and Mg-F pairs are only slightly left-shifted (<0.05 Å), and the estimated viscosity of the melt decreases from 4.613 mPa·s to 1.846 mPa·s with an increase in temperature from 1273 K to 1773 K, in agreement with the NNIP trained specifically for CaF_2-MgF_2. Our results provide valuable insights into the properties of the CaF_2-MgF_2 system at high temperatures and serve as predictive models for the development of new electrolytes that could be used for silicon epitaxy by adding silica.

1. Introduction

In recent years, the study of chloride and fluoride molten salt systems has gained notable attention due to their promising various industrial applications, including fuel solvent as well as coolant in the molten salt reactor (MSR), energy storage, and the electrolyte in solid oxide membrane (SOM) electrolysis for metal extraction processes, etc. Nevertheless, the high operation temperature and possible exposure of toxic gases to experimental personnel and corrosive damage to equipment have greatly hindered the study and development of molten salts [1].

Therefore, compared to the trial and error method of experimental testing, introducing the computational simulations not only saves time and costs but also efficiently carries out high-throughput calculations under a variety of representative conditions [2]. Computational methods such as molecular dynamics (MD) have been widely used to study the behavior of molten salt at elevated temperatures and to understand the interactions between ions or complex ion clusters in systems [3–5]. The classical MD or interatomic potential MD (IPMD) has the ability to simulate timescale in the range of hundreds of picoseconds (ps) or nanoseconds (ns) and thousands of atoms in a massive supercell at the same time to represent the bulk material. However, the accuracy of IPMD simulations depends on the choice of interatomic potentials, which describe the interactions between different ion pairs. Also, IPMD is limited to specific potential models for the pre-defined system. Therefore, researchers have come up with two approaches to overcome the above-mentioned problems: one is ab initio molecular dynamics

* Corresponding author.
E-mail address: yzhong@wpi.edu (Y. Zhong).
[1] Present Address: Chemical Science Division, Oak Ridge National Laboratory, P.O. Box 2008, Oak Ridge, TN 37831, USA.

https://doi.org/10.1016/j.commatsci.2024.113294
Received 10 July 2024; Received in revised form 9 August 2024; Accepted 11 August 2024
Available online 24 August 2024

(AIMD), which can be used to study the molten salt by solving the Schrodinger equation but requires significant computational resources and has limitations of simulation time and system size [6–8]; another, more recently, is machine-learning generated potentials called neural network interatomic potentials (NNIPs) that have emerged as a new promising class of machine learning potential model [9–12]. NNIPs are trained by large datasets of quantum mechanics calculations such as AIMD, which provide a high level of accurate information about energy and forces. After the training, it can be used to quickly predict these quantities without the need for additional AIMD simulations and shows higher flexibility over traditional interatomic potentials. However, such efforts are limited by the time required to generate new training data and re-train models for new systems, which can become quickly untenable for molten salt systems in which numerous corrosion products, fission species, and atmospheric impurities may exist. A recent effort that seeks to overcome this limitation is the development of a universal interatomic potential provided by Matlantis [13]. This application of Mantlantis has been introduced here, and the results between these three methods (AIMD, trained NNIP, and Mantlantis) have been compared. Matlantis is a versatile atomistic simulator that employs the potential of NNIPs and seamlessly integrates a deep learning model into a conventional atomic simulation framework. It facilitates extensive materials exploration through its capability to simulate the atomic-level characteristics of a wide range of materials. Also, it should be noted that Matlantis is a universally generalized predictor for all combinations of trained pseudopotentials, which is different from conventional NNIPs that have all been trained on a specific system.

For molten salts, both IPMD and AIMD simulations have been used extensively to study the behavior of chloride systems such as LiCl-KCl molten salt systems for decades and to better understand their basic thermodynamic properties and ion interactions under specific conditions [14–21]. In addition, LiF-NaF-KF (FLiNaK), LiF-BeF (FLiBe), and other fluoride systems have been studied because they are suitable for the coolant and solvent salt for the MSR [6,21–33]. KF-NaF-AlF_3 and LiF-NaF-AlF_3 systems have also been studied through MD for the large-scale production of aluminum [34–37]. Besides the above-mentioned chloride and fluoride systems, CaF_2-MgF_2 flux has attracted significant interest in the SOM electrolysis process with the yttria-stabilized zirconia (YSZ) membrane for magnesium, silicon and aluminum production [38–43]. Compared with the previous attempt of using mixing flux including barium fluoride, magnesium fluoride, and yttrium fluoride as the electrolyte to extract silicon crystals from silica [44,45], the CaF_2-MgF_2 system has many more advantages such as relatively low melting point, low toxic volatility, less corrosive to YSZ membrane, high silica solubility, and high ionic conductivity. However, understanding the structure and transport properties of CaF_2-MgF_2 and their temperature and composition dependence is challenging due to the scarcity of existing literature about experimental measurements and suitable interatomic potentials.

The goal of this study is to use the structural and dynamical properties investigation of the liquid CaF_2-MgF_2 binary system with its temperature dependence as the simplest case to test the capabilities, limitations, differences, and reliabilities between IPMD-NNIPs, AIMD, and Matlantis; then further high-ordered systems such as CaF_2-MgF_2-SiO_2 and their classical potential problems will be investigated in the future. We aim to probe the degree of structural disorder, thermodynamics properties, and ionic self-diffusivity in this system at temperatures above its melting point and to compare our results with existing experimental data. Additionally, we assessed and compared the strengths and limitations of three distinct simulation methods by analyzing selected results. In this paper, we will describe the methods used to generate the NNIPs, the simulation protocol and conditions, and the data analysis techniques. We will present and discuss the results of our simulations and relate them to the development of new applications for this system.

The present study offers a pioneering approach in the field of multiscale simulations by integrating Density Functional Theory (DFT)-based NNIPs with large-scale MD simulations using both the Matlantis framework using PreFerred Potentials (PFP) [63] and the Large-scale Atomic/Molecular Massively Parallel Simulator (LAMMPS) [46]. This combination enables accurate and systematic analysis of the structural and dynamical properties of the CaF_2-MgF_2 binary fluoride system, which is crucial for high-temperature applications in the molten salt industry. The novelty of this work lies in its ability to bridge disparate time scales and atomistic details, providing a comprehensive understanding of structural, thermodynamic, and transport properties across a wide range of temperatures and compositions. By meticulously validating and cross-verifying the results obtained from IPMD-NNIPs and Matlantis with AIMD data, this study ensures the reliability and robustness of the simulations. The significance of this research extends beyond the CaF_2-MgF_2 system, demonstrating a scalable and transferable methodology that can be applied to other complex materials systems, thereby advancing the capabilities of multiscale modeling in materials science.

2. Methods

2.1. AIMD

A supercell containing 96 atoms (16 Ca, 16 Mg, and 64F) was considered to represent the 50–50 mol% MgF_2-CaF_2 composition. AIMD simulations for this fluoride system were performed by the Vienna Ab-Initio Simulation Package (VASP) [47–49]. The Generalized Gradient Approximation (GGA) with the Perdew Burke Ernzerhof (PBE) was employed for the exchange–correlation energy [50]. Also, the Projector Augmented Wave (PAW) pseudopotentials were chosen for Ca ($3s^2 3p^6 4s^2$), Mg ($3s^2$), and F ($2s^2 2p^5$) [51,52]. The global energy cut-off for the plane wave was set to 600 eV, and 10^{-4} eV was used as the convergence criteria for the electronic self-consistent loops. Calculations were performed using a $1 \times 1 \times 1$ k-point and a time step of 2 femtoseconds (fs), which results in the convergence within 2 meV/atom. The methodology employed in this study involved utilizing the density functional theory (DFT-D3) formulation introduced by Grimme [53] to incorporate dispersion interactions. The canonical ensemble (NVT) was adopted, employing a Nosé-Hoover thermostat [54] to regulate temperature at 1400 K, while periodic boundary conditions were maintained throughout the simulations. With the aim of obtaining the relaxed density, 6 volumes were considered to fit the equation of state at 1400 K. For all volumes, in order to avoid atomic overlap in initial configurations, we used the Packmol package to generate random atomic positions in the supercell [55]. The initial volumes containing random configurations were equilibrated for at least 20 ps before obtaining average values of pressures to fit the equation of state. During the simulation, the total pressure of the system was averaged from nearly 50 ps trajectory at different volumes to fit the Birch-Murnaghan equation of state (EOS) [56]. According to our previous work, an equilibrated simulation trajectory of 50 ps should be sufficient to obtain converged molten-salt structure and properties [57]. Based on the resulting pressures and volumes at a given temperature, the fitted P-V curves were used to determine the equilibrium volume.

2.2. Training of NNIPs and IPMD

To train the NNIPs, the study utilized the DeePMD-kit (DP-kit) package version 1.3.3 [58]. Within the DP-kit, the Deep-Pot-Smooth Edition (DeepPot-SE) potential was selected for its ability to produce smooth and continuously differentiable surfaces of potential energy [59]. The DeepPot-SE model establishes a relationship between the local environment surrounding each atom within an 8 Å cut-off and the per-atom energy. This ensures that the collective sum of atomic energies aligns with the reference DFT energy. The gradients derived from NNIP-predicted energies are subsequently employed to compute atomic forces.

During the training of a DeepPot-SE model, the loss function is evaluated and minimized by incorporating both reference energies and forces, following the procedures of our previous study [11].

The training dataset comprised 17,500 relaxed configurations at 1400 K by using AIMD data with 96 atoms. In addition to these, 5473 with 15.76 % expanded and 6438 with 5 % compressed configurations at 1400 K were also included in the NNIP training. All training dataset configurations were obtained from AIMD calculations discussed in Section 2.1. Our previous work shows that a small percentage of expanded and compressed configurations were necessary to get stable densities using the trained NNIP [11,12]. The datasets were randomly divided into two parts: 80 % for training and 20 % for validation during the training procedure. The size of the embedding network is (25, 50, 100) where the fitting network is (240, 240, 240). And 2 Å and 8 Å were selected for the smooth and hard cut-off radius, respectively. During the training, the prefactors p_e^{start}, p_f^{start}, p_e^{limit}, and p_f^{limit} were pre-set to 0.002, 1000, 1, and 1 in the loss function. The above parameter settings have been verified to obtain the well-adjusted potential energy surface by our previous study for high-order molten salt system [11]. Only energies and forces from AIMD were used for training, and their errors for our trained potentials are 1.01 meV/atom and 36.6 meV/Å, which fall within the precision range of DFT and indicate the high accuracy of energy predictions during our testing.

The structural and dynamical properties of CaF_2-MgF_2 molten salt were investigated using IPMD simulations performed using the LAMMPS code [46]. Trained NNIPs were used to describe the interactions between different ion pairs. The simulations were performed in the isothermal-isobaric (NPT) ensemble [60–62] at temperatures of 1273–1773 K, and the time step was set to 0.001 ps. The initial configurations were obtained by first raising the temperature of the supercells to 5000 K and equilibrating the system for 100 ps, then gradually cooling to the desired temperature for a total of another 100 ps. Finally, the production runs were performed for the last 100 ps, and thermodynamic output data were collected every 0.1 ps. The supercell size was set to a total of 768 atoms (for eutectic composition: 128 Ca, 128 Mg, and 512 F), and periodic boundary conditions were applied.

2.3. Matlantis with PFP

Matlantis is powered by a universal neural network potential called PFP [63], which is trained from DFT calculations. It currently accommodates combinations involving 72 different elements, with plans to incorporate additional elements in the future. The speed of Matlantis can exceed 10,000 times faster than conventional DFT calculations with their pre-trained model and physical property library. No hardware or software dependencies and training data are needed from users. We performed MD simulations for the CaF_2-MgF_2 fluoride system in Matlantis from 1273 K to 1773 K at 50 mol% MgF_2 content. The initial configurations are the same as that in the IPMD part of Section 2.2, which contains a total of 768 atoms. We have collected thermodynamics data and trajectories during the 50 ps NVT production running for results analysis and comparison. The used force field, model version of estimator, and calculation model are PFP, v5.0.0, and EstimatorCalcMode.CRYSTAL_U0_PLUS_D3, respectively.

3. Results and discussion

In this part, we have presented the performance and implications of our trained potentials, the density profiles, and the derived structural information. Also, the physio-chemical properties, as well as an in-depth examination of diffusivities and viscosity in the context of our research objectives, are revealed through our analysis.

3.1. Density

The temperature dependence of density can be expressed as:

$$\rho = A + BT \tag{1}$$

ρ is g/cm^3, T is Kevin and A, B are fitting parameters. Detailed numbers are shown in Table 1. Fig. 1 shows the temperature dependence of calculated densities of the system from both IPMD-NNIPs, AIMD, and Matlantis for the eutectic composition of the CaF_2-MgF_2 system. Calculated densities are analyzed using averaged equilibrium volume through the NPT ensemble for all three methods and are plotted as solid lines, and found experimental values are shown as dashed lines. We also estimate the densities through the additive molar volume method, which assumes the system is totally ideal mixing [64]:

$$\rho_{ideal\ mix}(T) = \frac{\sum X_i M_i}{\sum X_i V_i(T)} \tag{2}$$

Where X_i and M_i are the mole fraction and molar mass of component i, and $V_i(T)$ is the molar volume of component i at temperature T. The empirical molar volumes for CaF_2 and MgF_2 salts are derived from the measurements of the pure components [65,66] and are given in Table 2. Considering the melting points of the pure CaF_2 and MgF_2 salts and their eutectic mixing are 1683 K, 1525 K and 1253 K [67], respectively, it can be assumed that the given empirical molar volumes of the pure components at 873 K and 1073 K can be used to estimate their mixed solid densities below the eutectic temperature.

Compared with the AIMD simulations without dispersion correction, the absolute values of calculated densities from simulations by using the DFT-D3 dispersion method have a much better agreement with the additive molar volume method and the existing experimental results. However, the results from IPMD with NNIPs (trained on DFT-D3 AIMD data) show a 5–10 % error, the same as those without dispersion, and the equilibrium volumes from Matlantis are much larger than others. One possible reason is that Matlantis is a generalized potential that has not previously been trained on our system; also, since the dispersion correction on DFT is semi-empirical and typically needs to be tested depending on the system, the same corrections are likely not represented in the Matlantis training set. Another reason for the general underprediction of the NNIP is the loss of information beyond the finite-range cutoff (here, 8 Å), which could result in error in representing long-range electrostatic interactions that are present in molten salt [11,68]. Even though there are some discrepancies between the absolute values, the fitted slopes of temperature dependencies are very close to each other and the experimental values. Considering the equilibrium volumes are critical and will have a large effect on subsequent property estimations during the NVT calculations, the resulting volumes and structures from IPMD-NNIPs and Matlantis have been re-sized to the fitted configurations from the AIMD EOS process for further production runs.

Table 1
Fitted parameters of A and B.

Methods	A ($g \bullet cm^3$)	B ($\times 10^{-4}$ $g \bullet cm^3 \bullet K^{-1}$)	Temperature range (K)
PFP_NPT	2.8995	−4.6970	1273–1773
AIMD_NPT (No dispersion)	3.0657	−4.5205	1273–1573
AIMD_NPT (DFT-D3 dispersion)	3.1441	−4.2767	1273–1673
AIMD_EOS (DFT-D3 dispersion)	3.1855	−4.5124	1273–1773
IPMD-NNIPs_NPT	3.1325	−4.7915	1273–1773
Additive Molar Volume Method (Ideal mixing) [65,66]	3.2112	−4.5611	873–2100
1989, Shigeta HARA et al. [69]	3.3120	−4.8300	1670–1854
2018, Michal Korenko et al.[70]	3.2907	−4.7480	1273–1353

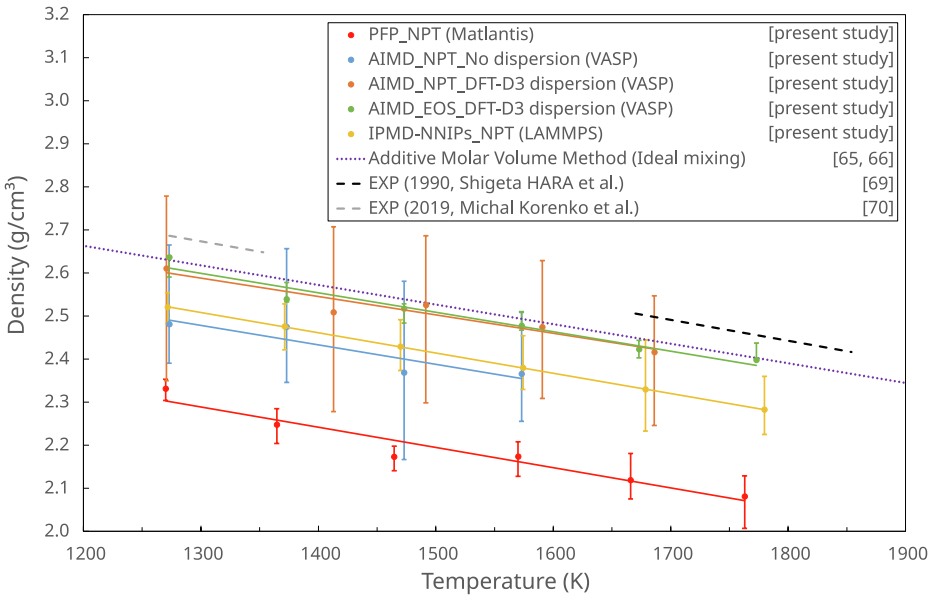

Fig. 1. Density comparison between AIMD, IPMD-NNIPs, and PFP for the eutectic composition of the CaF_2-MgF_2 system.

Table 2
The empirical molar volumes for the pure CaF_2 and MgF_2 salts [65,66].

Standard Empirical Molar Volume ($cm^3 \bullet mol^{-1}$)	873 K	1073 K	1700 K	1800 K	1900 K	2000 K	2100 K
Pure CaF_2 salt	27.5	28.3	31.06	31.55	32.06	32.58	33.12
Pure MgF_2 salt	22.4	23.3	26.58	27.19	27.82	28.49	29.19

3.2. Structural information

Here, the results at 1773 K are demonstrated as an example; the results for other temperatures (1273 K–1773 K) can be found in the Supplemental Materials.

3.21. Radial distribution function (RDF)

The partial RDFs of different ion pairs $g_{ij}(r)$ at 1773 K with eutectic composition from IPMD-NNIPs (DeepMD-LAMMPS), AIMD (VASP), and PFP (Matlantis) are all calculated using in-house Python code with a third-party library named vasppy [71] and shown in Fig. 2 for comparison. The y-axis of $g_{ij}(r)$ presents the probability of finding a particle at a distance r from the particle at the origin and is given by:

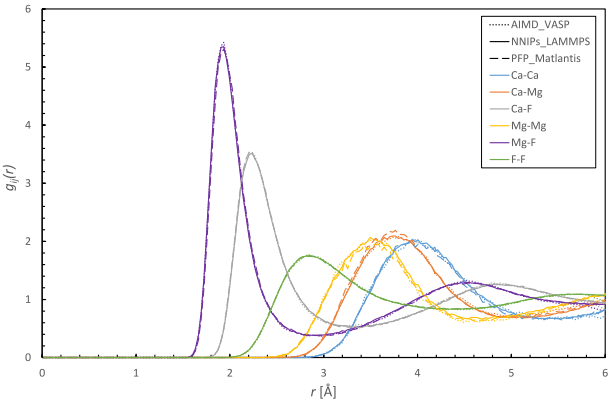

Fig. 2. Partial RDFs of different ionic pairs of eutectic CaF_2-MgF_2 system at 1773 K by AIMD, NNIPs, and PFP in this work.

$$g_{ij}(r) = \frac{V}{N_j N_j} \sum_j \frac{\langle n_{ij}(r, \Delta r) \rangle}{4\pi r^2} \quad (3)$$

The V represents the total volume of the simulated supercell, while N denotes the quantity of particles present. $n_{ij}(r, \Delta r)$ stands for the mean count of atom j that encircles a central atom i within a specified proximity range of Δr.

Therefore, the corresponding radius of the first peak indicates the average bond length between a pair of two kinds of ions. Table 3 gives the averaged bond lengths for the Ca-F and Mg-F pairs at 1773 K by using the above three methods. It is easy to find that the estimated average bond lengths are almost the same from three different simulation methods for each pair, and the heights are also very close except for the cation-cation pairs, which have some slight differences.

3.22. Temperature dependency of RDF

We also studied the temperature dependency of RDF for counter-ion pairs. As we can see in the zoom-in figures of the first peak from PFP (Matlantis) results in Fig. 3, the first peak height gradually decreases from 3.843 to 3.556 and from 5.772 to 5.309 with temperature increasing for both Ca-F and Mg-F pairs, respectively, which indicates the system is becoming more disordered as the temperature rises. This is attributed to the higher kinetic energy of ions at elevated temperatures,

Table 3
Calculated averaged bond length of cation–anion pairs at 1773 K.

Pair	Ca-F			Mg-F		
Method	AIMD	NNIPs	PFP	AIMD	NNIPs	PFP
Averaged bond length (Å)	2.205	2.235	2.235	1.935	1.935	1.935

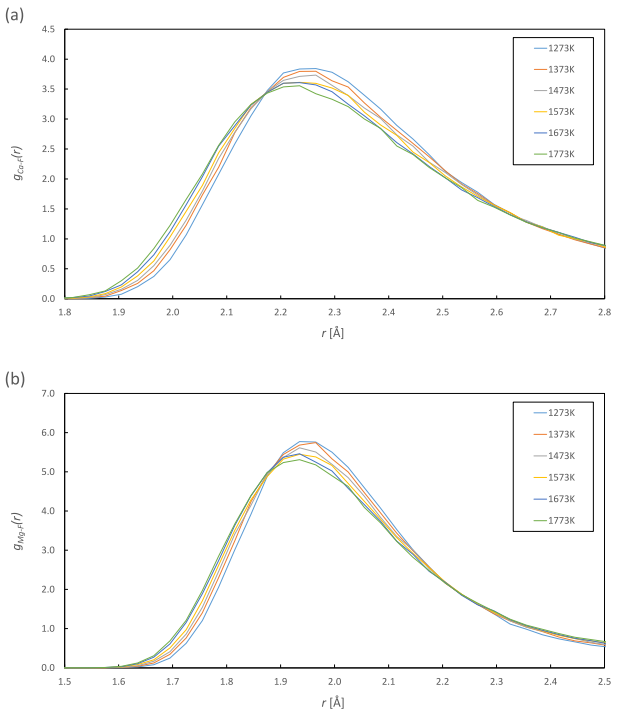

Fig. 3. The temperature dependency of the height and position of the first peaks from PFP (Matlantis) results for (a) Ca-F and (b) Mg-F in this work.

which weakens the bond strength. In addition, the position of the peak, or estimated average bond length, is also subtly left-shifted from 2.265 Å to 2.235 Å for Ca-F pairs. For Mg-F bond length, even though our raw data shows a constant value of 1.935 Å for all temperatures due to the large interval of 0.03 Å of distance *r*, it is easy to find that the peak is also left-shifted in the figure.

This phenomenon is evident across all three different methods and detailed comparisons of partial RDFs and average bond lengths at various temperatures obtained from AIMD, NNIPs, and PFP are provided in Supplemental Materials Figure S1 and Table S1.

3.23. Coordination number (CN)

The coordination number (CN) of different ion pairs can be estimated from the integral of partial RDFs, and the first shell CN is analyzed by integrating the area from the origin to the first minimum of the curve [72]. The CN results at 1773 K are shown in Fig. 4 and Table 4. Given the cutoff at the first minimum in partial RDFs, the CN for Ca-F and Mg-F pairs are around 7 and 5.5, respectively. Additionally, as temperature increases, the CN tends to decrease slightly, as shown in Supplemental

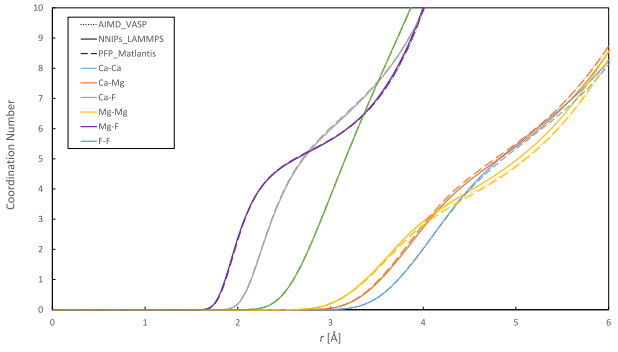

Fig. 4. The calculated coordination number of different ionic pairs of eutectic CaF_2-MgF_2 system at 1773 K from AIMD, NNIPs, and PFP.

Table 4
The first shell CN of cation–anion pairs at 1773 K from AIMD, NNIPs, and PFP.

	Ca-F		Mg-F	
	cut-off	CN	cut-off	CN
AIMD_VASP	3.255	6.675	2.985	5.594
NNIPs_LAMMPS	3.375	7.085	2.865	5.387
PFP_Matlantis	3.345	7.022	2.955	5.559

Materials Figure S2 and Table S2. This is due to the same reason discussed in the RDF part that higher temperatures will weaken the bond strength. Consequently, the central cations are less able to attract and hold anions.

In Fig. 5, the polyhedron analysis was conducted for the final step at 1773 K in the IPMD-NNIPs simulation. Most of the polyhedra with Ca as the center atom are connected to 7 F ions, and for the Mg-centered polyhedron, we also found that there is not much difference between the probability for Mg to connect to 5 and 6 F ions, which is consistent with the CN results we obtained.

3.24. Angular distribution functions (ADF)

The angular distribution functions (ADF) have also been analyzed at 1773 K and shown in Fig. 6. The ADF describes the probability distribution of bond angles or dihedral angles within a molecular system. It helps us to understand the geometry and predict the coordination numbers, as well as the potential clusters and their connectivity. The 2D density plots between the $\theta_{Cation-F-Cation}$ and the distance of Cation-Cation are present in Fig. 7.

Based on the resulting ADF Figs. 6 and 7:

1. The results from three different methods are consistent with each other, especially for the position of peaks. However, for the angle of the Mg-F-Mg pair, the result from NNIPs shows a sharper peak and lower frequency in the small angle range than the other two methods. This is probably caused by different cutoff selections of bond length. Fortunately, the frequency of ADF just indicates the probability of finding a specific angle and what we care more about is the angle or position of the peak.
2. Both Ca-centered and Mg-centered angles (F-Ca-F and F-Mg-F) have a significant peak at a lower angle and a secondary peak at a

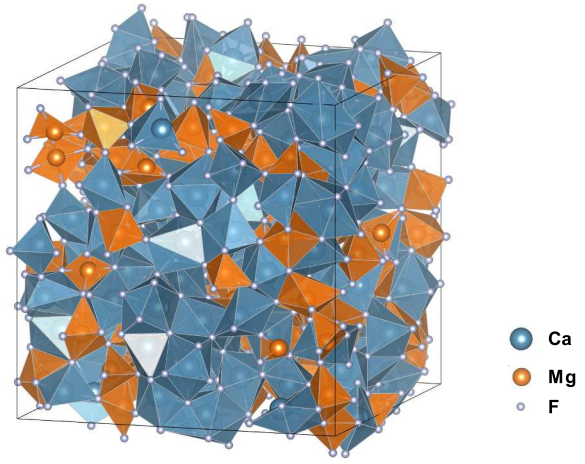

Fig. 5. The polyhedron analysis for the final step at 1773 K from IPMD-NNIPs; Ca, Mg and F ions are colored blue, orange, and gray, respectively. (For interpretation of the references to colour in this figure legend, the reader is referred to the web version of this article.)

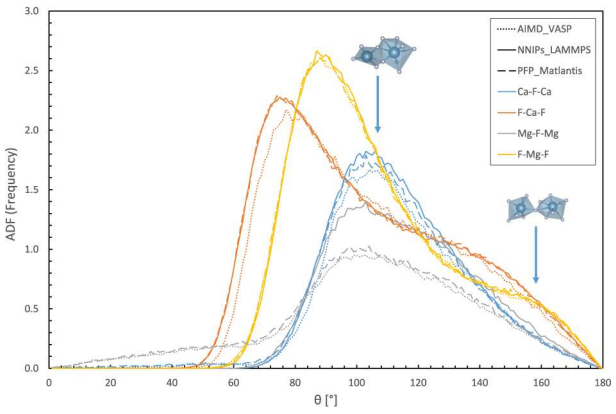

Fig. 6. The analyzed angle distribution function of the counter-ion pairs at 1773 K from AIMD, NNIPs, and PFP.

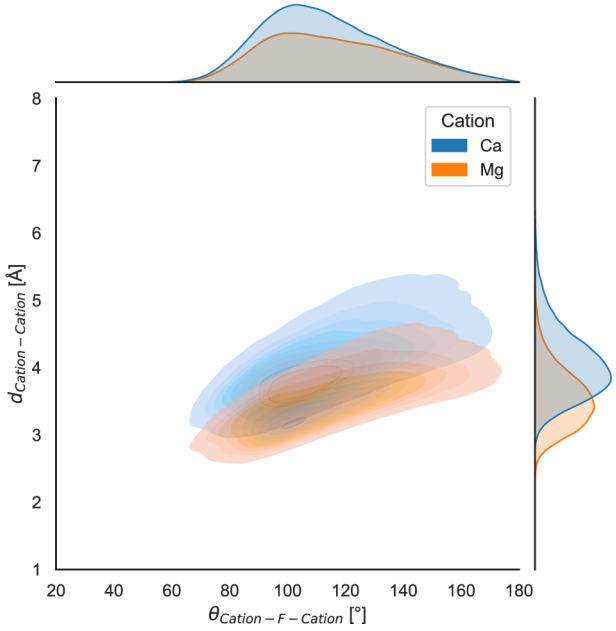

Fig. 7. Cation-F-Cation bond angle distributions from PFP at 1773 K.

higher angle. The lower angle and higher angle represent two adjacent and two opposite F ions within the cation-centered polyhedron.
3. As for the F-centered angle, the lower the angle, the higher the probability for linked cations re-connected by another F ion, thus making two neighboring cation-centered polyhedrons share two or even three F ions, as known as edge-sharing and face-sharing. Similarly, the high F-centered angle implies two adjoining cation-centered clusters connect with only one F ion, which is corner-sharing. Since the repulsive force between the F ions, the F-centered angle starts from around 70 degrees. From Fig. 6, we found the peak of F-centered pairs located at 103 degrees and 100 degrees for Ca-F-Ca and Mg-F-Mg pairs. Also, these two F-centered pairs have lower frequency with increasing angle, which means most adjacent polyhedrons are more likely to be connected with edge-sharing or face-sharing rather than corner-sharing.
4. In Fig. 7, the single high-density region indicates the edge-sharing complexes are dominant for both of Ca and Mg cations. The Mg region is located at relatively lower cation-cation distances compared to the Ca region; this is also consistent with the smaller average calculated bond length of Mg-F in Section 3.21.

The comparison of analyzed ADF for the counter-ion pairs at various temperatures between AIMD, NNIPs, and PFP can be found in Supplemental Materials Figure S3.

3.3. Heat capacity

The heat capacity is the ability to absorb heat as temperature increases and can be calculated at constant volume conditions by:

$$C_V = \left(\frac{dU}{dT}\right)_V \approx \left(\frac{\Delta E}{\Delta T}\right)_V \tag{4}$$

U is the internal energy, and E is the total system energy. Since the methods of evaluating system energy are different between the methods (AIMD, NNIPs, and PFP), the direct comparison of total system energy values is meaningless and unnecessary. However, the heat capacity is only related to the slope of enthalpy that follows temperature changes, which makes it comparable.

The calculated average C_v are 0.907 $J{\cdot}K^{-1}{\cdot}g^{-1}$, 0.947 $J{\cdot}K^{-1}{\cdot}g^{-1}$, 1.121 $J{\cdot}K^{-1}{\cdot}g^{-1}$ for AIMD, NNIPs, and PFP, respectively. The results from all three methods are very close and consistent with each other.

3.4. Ionic self-diffusivity

The mean square displacement (MSD) can be extracted and calculated from the trajectory files during the MD simulations. It is given by:

$$MSD(t) = \langle \Delta r^2(t) \rangle = \frac{1}{N}\sum_{i=1}^{N}[r_i(t) - r_i(0)]^2 \tag{5}$$

Where N is the total number of atoms, $r_i(t)$ is the position of the particle i at time t, $r_i(0)$ is the initial position of the particle i. The MSDs of the individual elements (Ca, Mg, and F) of the eutectic CaF_2-MgF_2 system at 1773 K are shown in Fig. 8 for comparison. Note that the MSD results from AIMD end at 20 ps. All MSD curves increase linearly with time, indicating that the ions are diffusing in the liquid. Fig. 8 shows that the ions of both Ca and Mg have a similar degree of mobility with no significant differences, but F ions have a greater slope that indicates larger diffusivities.

The ionic self-diffusivities were able to be calculated using the Einstein equation for Ca, Mg, and F ions at the above condition:

$$D = \frac{1}{3}\lim_{t\to\infty}\frac{d}{dt}(MSD) \tag{6}$$

The Einstein equation suggests the diffusivity can be estimated by the slope of MSD versus time, then divided by 3 due to the ion diffusing along the x, y, and z three directions. The results at 1773 K are shown in Fig. 9.

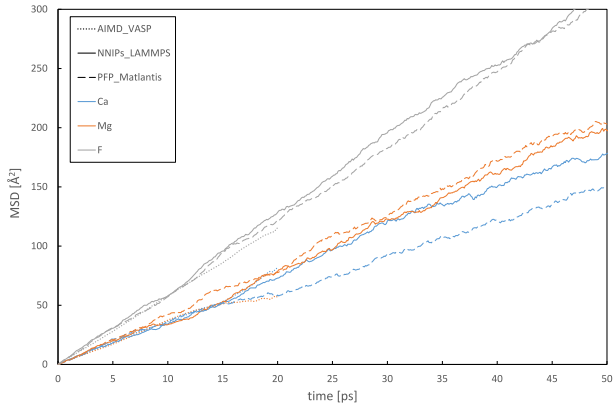

Fig. 8. The MSDs comparison for Ca, Mg, and F ions at 1773 K between AIMD, NNIPs, and PFP (AIMD results end at 20 ps).

The error bars presented in Fig. 9 represent the statistical uncertainties in the diffusivity calculations. These uncertainties arise from several factors during the simulation and data analysis process. First, diffusivity calculations are based on averaging the MSDs over multiple time intervals and ion trajectories; the inherent fluctuations in these measurements contribute to the overall uncertainty. Second, longer simulations generally provide more accurate results but are computationally expensive; shorter simulations can introduce higher uncertainty due to limited sampling, especially for the AIMD_VASP results. Last, we have conducted multiple independent simulation runs to obtain a statistically significant estimate of diffusivity; the error bars reflect the standard deviation of diffusivity values obtained from these independent runs.

Compared to the NNIPs and PFP methods, AIMD results exhibit significant uncertainty and longer error bars. This is because, considering the time and computational cost efficiency, there are only one-eighth the number of atoms in AIMD supercells compared to the supercells in NNIPs and PFP. Fewer atoms result in high discrepancies during the time average process for calculating MSDs, thus affecting the diffusivities. However, overall, for each element, all three methods provided similar predictions. As we discussed in the MSDs part, the diffusivities of Ca and Mg ions are very close to each other, and the F ions have the highest self-diffusivity. In addition, the diffusivity of F ions is only around twice that of cations. The possible reason that F ions didn't diffuse much faster is the ionic radius of Fluorine is almost the same as Calcium and even bigger than Magnesium, which makes it harder for some F ions with relatively low kinetic energy to cross the energy barrier and diffuse freely, thus lower the total average self-diffusivity of F ions. The differences between temperatures and among the three methods are shown in Supplemental Materials Figure S4.

The Arrhenius diagram is also investigated and plotted in Fig. 10 to obtain the temperature relationships and the activation energies. Based on the calculated diffusivities, activation energies of diffusion can be derived by taking the natural logarithm of both sides of the Arrhenius equation:

$$lnD = -\frac{Q_{dif}}{R}\left(\frac{1}{T}\right) + lnD_0 \tag{7}$$

R is gas constant, Q_{dif} is the activation energy of diffusion, T is temperature, and D is the self-diffusivity. The similar activation energy of cations and anions, as listed in Table 5, indicates they experience comparable barriers to movement within the salt at high temperatures.

3.5. Viscosity

Viscosity is a fundamental property of fluids that characterizes their resistance to flow. Since the AIMD is not able to get long enough trajectories to use the Green-Kubo taking autocorrelation of the stress tensor, another feasible method to estimate the approximate viscosity from MD simulations is using the Stokes-Einstein equation, and is given by:

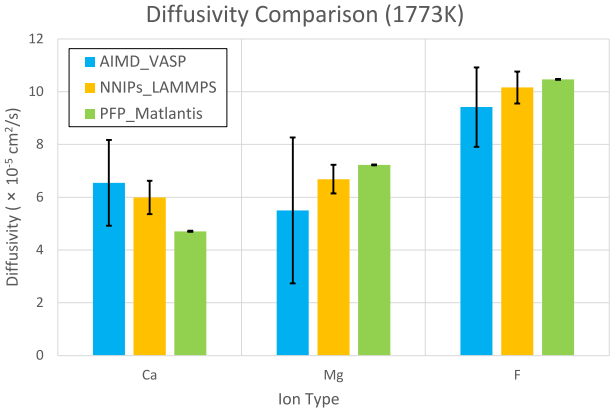

Fig. 9. Comparison of calculated diffusivities for Ca, Mg, and F ions with eutectic CaF_2-MgF_2 system at 1773 K from AIMD, NNIPs, and PFP.

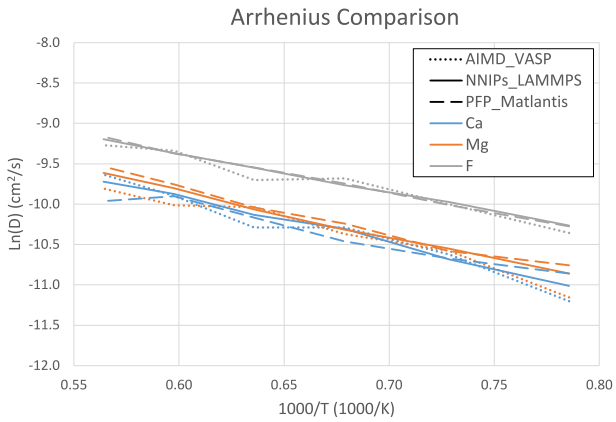

Fig. 10. Comparison between AIMD, NNIPs, and PFP for Arrhenius diagram of diffusivity.

$$\eta = \frac{k_B T}{2\pi \bar{D} d} \tag{8}$$

Where k_B is the Boltzmann constant, and T is the temperature. $\bar{D}$ is calculated by the arithmetic mean of self-diffusion coefficients of Ca^{2+}, Mg^{2+}, and F^- ions. And d is the radius of the spherical particle, which is approximately considered as the averaged bond length of all ionic pairs in molten salt CaF_2-MgF_2:

$$d = \frac{d_{Ca-Ca} + d_{Mg-Mg} + d_{F-F} + 2d_{Ca-F} + 2d_{Mg-F} + 2d_{Ca-Mg}}{9} \tag{9}$$

There is another method called reverse non-equilibrium MD (rNEMD) [73]. It can also predict viscosity and can be easily conducted through the Matlantis feature package. During the rNEMD, an artificial velocity gradient is generated between the bottom and middle (along the z direction) in the simulation box. Then, the exchanged momentum can be defined as the momentum difference along the x direction between the bottom and middle:

$$P_{exchanged} = P_{x,bottom} - P_{x,middle} \tag{10}$$

The momentum flux is proportional to the product of viscosity and velocity gradient:

$$\frac{\sum P_{exchanged}}{2tS_{xy}} = \eta \frac{\partial v_x}{\partial z} \tag{11}$$

t is time, S_{xy} is the area of the x-y plane of the simulation box, v_x is the partial velocity along the x direction, and η is the viscosity.

As shown in Fig. 11, with the temperature rising from 1273 K to 1773 K, the calculated viscosity η of eutectic CaF_2-MgF_2 molten salt drops from 4.836 mPa·s to 1.872 mPa·s, 4.088 mPa·s to 1.764 mPa·s, and 3.877 mPa·s to 1.792 mPa·s estimated by the Stokes-Einstein equation from AIMD, IPMD-NNIPs, and PFP, respectively. In addition, the viscosity predicted by the rNEMD method also drops from 4.613 mPa·s to 1.846 mPa·s, which is consistent with the above results. However, Michal Korenko et al. [70] have reported that their measured averaged viscosity for the 49.6 % CaF_2 – 50.4 % MgF_2 system dropped from 7.822 mPa·s to 5.730 mPa·s and the experimental condition is from 1000 °C to 1080 °C, which is around 1.5 times higher than our prediction in the same temperature range but within reasonable approximation. Besides, our simulations are much closer to their additive model results.

The deviation can be attributed to several factors inherent to the

Table 5
The predicted diffusion pre-factor D_0 and activation energy Q_{dif} of self-diffusivity of Ca, Mg, and F ions.

Species	Ca			Mg			F		
Methods	AIMD	NNIPs	PFP	AIMD	NNIPs	PFP	AIMD	NNIPs	PFP
D_0 ($\times 10^{-5}$ cm^2/s)	250.19	169.83	69.24	152.51	157.01	167.16	149.03	150.01	168.75
Q_{dif} (kJ/mol)	54.13	48.86	38.26	47.99	46.79	46.97	40.19	39.79	41.25

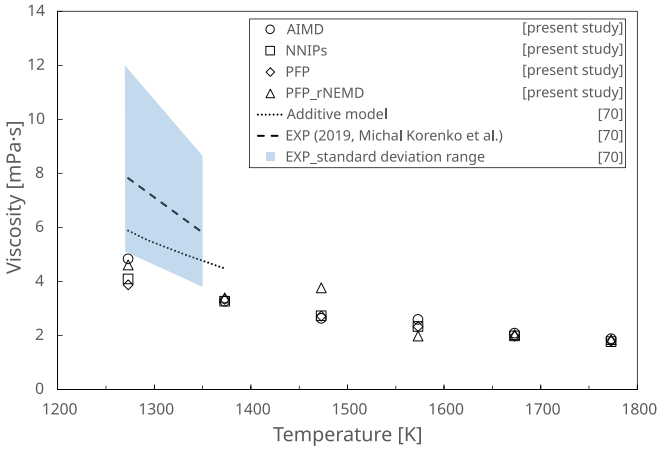

Fig. 11. Calculated viscosity and its temperature dependence of eutectic CaF_2-MgF_2.

nature of MD simulations. On one hand, the accuracy of the interatomic potentials used plays a crucial role in determining the viscosity. While these potentials are trained and validated, slight inaccuracies or limitations in capturing long-range interactions or complex atomic behaviors can result in deviations. On the other hand, the finite size of the simulated system and the boundary conditions applied can also affect the viscosity measurements. In smaller systems, boundary effects and finite-size effects are more pronounced, leading to deviations in the calculated viscosity.

4. Discussion

By comparing the density results between IPMD-NNIPs, AIMD, and Matlantis, a significant difference is that the equilibrium volumes are overestimated from Matlantis. One possible reason for this is that the PFP potentials are trained from ab initio calculations, most of which are conducted at much lower temperatures or at 0 K. As such, configurations sampled at higher temperatures are likely to deviate more from the training set, resulting in a larger difference in equilibrated volumes under the NPT ensemble. Furthermore, training data used for PFP likely includes different approximations for dispersion interactions in order to fit a wide range of chemical systems. Here, the density is sensitive to small deviations in predicted energy and dispersion interactions. As a result, the Matlantis overestimated lattice volume by at least 14 % compared to existing values in literature, and 5–10 % error for that of IPMD-NNIPs results. This proved our trained in-house potential is more accurate than the universal PFP potentials in Matlantis during averaging equilibrium volumes in the NPT ensemble for this specific CaF_2-MgF_2 molten system. The overestimated lattice volume will have large effects on subsequent properties determination, such as causing longer average bond lengths between ions, thus right-shifting peaks in the RDF results and decreasing the energy barrier of diffusion because of more interstitial spaces. Therefore, we have re-sized all NPT resulting supercells in AIMD, IPMD-NNIPs, and Matlantis to the equilibrium volumes obtained from the EOS procedure in AIMD to have a fair comparison of accuracy before the NVT production run.

From the comparison of lattice and structure analysis, all three methods showed almost the same outputs, especially for the RDF and CN analysis. Even though there are some discrepancies in the frequency of the Mg-F-Mg pair in ADF evaluation, the positions of major peaks are consistent with each other. This kind of difference won't affect the conclusion that neighboring polyhedrons prefer to be linked through more than one F ion. After the transport properties study of ionic self-diffusivity, closed values of activation energies are obtained from three different methods. However, AIMD gives larger error bars in diffusivity investigations because of the limitation of low efficiency of time and computational cost. As for the viscosity, our simulation results show a negative deviation from the experiments but relatively close to the prediction from the additive model [70]. These discrepancies can also be explained by the volume difference in our density comparison. The equilibrium volumes we used for final production runs were only 0.73 % larger than that of the additive model but 2.68 % and 3.15 % larger than that of two experimental data from the literature [69,70]. This is consistent with previous work in predicting the viscosity of LiF-BeF_2 mixtures, in which a similar deviation was found with different cell sizes [12]. The discrepancy in results exists since we didn't directly use the volumes in experiments, and herein, we want to find a simulation method that can give the most accurate predictions of equilibrated volumes. Although earlier studies have reported simple eutectic systems, it is quite challenging to conduct the proper experiments for higher-order systems, e.g., systems containing CaO/MgO and SiO_2 [70].

Based on the comparison of the above results, and considering the capability to handle the massive number of atoms and requires less computational resources, the calculated properties from IPMD-NNIPs and Matlantis with PFP are reasonably acceptable and would be able to represent the bulk materials comparable to the first-principal predictions and experiments, as long as given the determined equilibrium volumes. However, IPMD-NNIPs also have their limitations, such as system dependence and still requiring ab initio calculation inputs as the training data. On the other hand, the Matlantis platform provides an alternative solution for the high-order system with pre-trained and universal potentials. It will greatly reduce the difficulty of investigating much more complex systems with the capability of longer-time MD simulations. Another application of Mantlantis could be used for rapid sampling configurations to accelerate the development of NNIPs. Due to the speed (several orders of magnitude faster) and scalability (linear with system size) of Matlantis relative to AIMD, a more diverse set of configurations can be generated, subsampled and labeled, maximizing the representativeness of training set and robustness of NNIP models. This would address a key bottleneck of trained NNIPs in which training sets are developed with AIMD simulations that generate large amounts of correlated data. Conversely, transfer learning could be employed to update the Matlantis model using system-specific data to fine-tune the model, which would allow a more accurate model with minimal additional DFT data. However, such functionality is not yet available in the current Matlantis software.

In summary, Matlantis has the ability to conduct high-speed simulations, but it is critical to obtain accurate thermodynamic values from the appropriate volume and structure. If proper relaxation lattice is given through experiments or EOS procedures, IPMD-NNIPs and Matlantis will have enough accuracy comparable to the density function theory calculations with the advantage of time and cost.

5. Conclusions

This study used a combination of IPMD-NNIPs and AIMD simulations to investigate the properties of the CaF_2-MgF_2 fluoride system at high temperatures, and the Matlantis with universal PreFerred Potentials was introduced to evaluate its capability and accuracy for molecular dynamics simulations and calculated physio-chemical properties. The use of NNIPs in this study has allowed us to perform large-scale MD simulations on a system that would be computationally expensive to simulate using ab initio methods. The structural properties of the system were analyzed using the radial distribution function (RDF), which showed that the two components are well mixed, with no signs of short-range order or complex ion cluster formation. Additionally, we calculated the specific heat capacity through the above three methods. The MSDs and ionic self-diffusivities were analyzed and compared using the Einstein relation and rNEMD method. The Arrhenius diagrams are plotted to compare the activation energy of Ca, Mg, and F ions. Based on the comparison of viscosity results between our simulations, experiments and additive model, the equilibrium volumes estimated by the EOS procedure can be accepted with less than 4 % error and used for higher order and more complex systems which may not have enough information from existing literature and hard to scale because of severe experimental conditions.

Despite the robustness and innovative aspects of our methodology, several limitations and potential sources of error should be acknowledged. The accuracy of NNIPs and Matlantis potentials is crucial for reliable simulations. While these potentials are trained on extensive datasets, they may still have limitations in capturing all possible atomic interactions, especially under varying temperature and pressure conditions. Any discrepancies in the potential can directly impact the accuracy of the simulation results. Maintaining precise control over temperature and pressure in MD simulations is challenging. Small fluctuations can lead to significant deviations in computed properties like diffusivity and viscosity. These fluctuations are a source of error that can affect the reliability of the results. The simulations were performed for finite time periods and system sizes due to computational resource constraints. Longer simulations and larger system sizes could potentially provide more accurate results by reducing statistical errors and better representing macroscopic properties. However, they are often limited by available computational power, especially for AIMD.

Overall, the results of this study provide new insights into the behavior of the CaF_2-MgF_2 molten salt system at high temperatures and support the potential of this material for use in high-temperature applications such as electrodeposition. The good agreement between the IPMD-NNIPs results, AIMD calculations, and the Matlantis outputs indicates that the Matlantis with PFP model used in this study is an accurate and reliable method for studying the properties of this system. The Matlantis could be considered as an alternative and useful MD simulation tool, especially for the higher-order complex system that requires fully developed interatomic potentials for IPMD or extreme time and computational resource costs for AIMD.

Author Contributions

Yifan Zhang conducted the literature review, conceived the study, collected and analyzed the data, interpreted the results, and wrote the initial draft of the manuscript. Rajni Chahal and Stephen Lam contributed to the methodology of the NNIPs, provided guidance and technical support for data analysis, and revised the manuscript. M Mustafa Azeem, Karl Ludwig and Michael C. Gao critically reviewed and edited the manuscript. Uday Pal and Adam Powell contributed to the conceptualization of the study. Yu Zhong supervised the project, secured funding, and provided critical feedback throughout the research process. All authors read and approved the final version of the manuscript.

CRediT authorship contribution statement

Yifan Zhang: Writing – original draft, Visualization, Validation, Methodology, Investigation, Formal analysis, Data curation. **Rajni Chahal:** Writing – review & editing, Visualization, Formal analysis. **M Mustafa Azeem:** Writing – review & editing. **Stephen Lam:** Writing – review & editing, Formal analysis. **Karl Ludwig:** Writing – review & editing. **Uday Pal:** Writing – review & editing, Conceptualization. **Michael C. Gao:** Writing – review & editing. **Adam Powell:** Writing – review & editing, Conceptualization. **Yu Zhong:** Writing – original draft, Visualization, Validation, Methodology, Investigation, Formal analysis, Data curation.

Declaration of competing interest

The authors declare that they have no known competing financial interests or personal relationships that could have appeared to influence the work reported in this paper.

Data availability

Data will be made available on request.

Acknowledgments

This research at Worcester Polytechnic Institute, Boston University, and University of Massachusetts-Lowell was supported by the US Department of Energy (DOE) NEUP program Award DE-NE0008937 and DE-NE0009204, Solar Energy Technologies Offices Award DE-EE0008988, and the US National Science Foundation (NSF) Award No. CMMI-1937818 and CMMI 1937829. In addition, we would like to acknowledge the computing resources from the Advanced Cyberinfrastructure Coordination Ecosystem: Services & Support (ACCESS) program Award: TG-DMR190004 and the technical support from the Academic & Research Computing team at Worcester Polytechnic Institute, especially James Leonard Kingsley and Siamak Mohammed Z. Najafi.

Appendix A. Supplementary data

Supplementary data to this article can be found online at https://doi.org/10.1016/j.commatsci.2024.113294.

References

[1] S. Delpech, et al., Molten fluorides for nuclear applications, Mater. Today 13 (12) (2010) 34–41.
[2] O. Beneš, R.J.M. Konings, Thermodynamic Calculations of Molten-Salt Reactor Fuel Systems, in: Molten Salts Chemistry, Elsevier, 2013, pp. 49–78.
[3] M. Salanne, et al., Calculation of activities of ions in molten salts with potential application to the pyroprocessing of nuclear waste, J. Phys. Chem. B 112 (4) (2008) 1177–1183.
[4] S. Wang, et al., Effect of MCl3 (M=La, U or Sc) component on the local structures and transport properties of LiCl–KCl–MCl3 eutectic: a molecular dynamics study, Electrochim. Acta 306 (2019) 366–376.
[5] L.B. Skinner, et al., Molten uranium dioxide structure and dynamics, 2014, pp. 984–987.
[6] H.O. Nam, et al., First-principles molecular dynamics modeling of the molten fluoride salt with Cr solute, J. Nucl. Mater. 449 (1–3) (2014) 148–157.
[7] S.T. Lam, et al., The impact of hydrogen valence on its bonding and transport in molten fluoride salts, J. Mater. Chem. A 9 (3) (2021) 1784–1794.
[8] Q.-J. Li, et al., Complex Structure of Molten NaCl–CrCl3 Salt: Cr–Cl Octahedral Network and Intermediate-Range Order, ACS Appl. Energy Mater. 4 (4) (2021) 3044–3056.
[9] S.-C. Lee, et al., Comparative studies of the structural and transport properties of molten salt FLiNaK using the machine-learned neural network and reparametrized classical forcefields, J. Phys. Chem. B 125 (37) (2021) 10562–10570.
[10] Y. Shi, S.T. Lam, T.L. Beck, Deep neural network based quantum simulations and quasichemical theory for accurate modeling of molten salt thermodynamics, Chem. Sci. 13 (28) (2022) 8265–8273.
[11] R. Chahal, et al., Transferable deep learning potential reveals intermediate-range ordering effects in LiF–NaF–ZrF_4 molten salt, JACS Au 2 (12) (2022) 2693–2702.

[12] A. Rodriguez, S. Lam, M. Hu, Thermodynamic and transport properties of LiF and FLiBe molten salts with deep learning potentials, ACS Appl. Mater. Interfaces 13 (46) (2021) 55367–55379.
[13] Matlantis (https://matlantis.com/), software as a service style material discovery tool.
[14] W. Zhou, J. Zhang, Chemical diffusion coefficient calculation of U3+ in LiCl-KCl molten salt, Prog. Nucl. Energy 91 (2016) 170–174.
[15] A. Bengtson, et al., First-principles molecular dynamics modeling of the LiCl–KCl molten salt system, Comput. Mater. Sci 83 (2014) 362–370.
[16] J. Wu, et al., The influence of NaCl concentration on the (LiCl-KCl) eutectic system and temperature dependence of the ternary system, J. Mol. Liq. 253 (2018) 96–112.
[17] F. Lantelme, P. Turq, Ionic dynamics in the LiCl–KCl system at liquid state, J. Chem. Phys. 77 (6) (1982) 3177–3187.
[18] J. Wang, et al., Molecular Dynamics Simulations of the Local Structures and Transport Coefficients of Molten Alkali Chlorides, J. Phys. Chem. B 118 (34) (2014) 10196–10206.
[19] M. Liu, P. Masset, A. Gray-Weale, Solubility of sodium in sodium chloride: a density functional theory molecular dynamics study, J. Electrochem. Soc. 161 (8) (2014) E3042–E3048.
[20] J. Song, et al., Towards the calculations of redox potentials in molten LiCl-KCl eutectic by ensemble averages based on first principles molecular dynamics, Electrochim. Acta 248 (2017) 462–469.
[21] H.O. Nam, D. Morgan, Redox condition in molten salts and solute behavior: A first-principles molecular dynamics study, J. Nucl. Mater. 465 (2015) 224–235.
[22] J. Xi, et al., Corrosion of Si, C, and SiC in molten salt, Corros. Sci. 146 (2019) 1–9.
[23] T. Asada, Y. Yamada, K. Ito, The estimation of structural properties for molten CaO–CaF2–SiO2 system by molecular dynamics simulations, ISIJ Int. 48 (1) (2008) 120–122.
[24] M. Salanne, et al., Heat-transport properties of molten fluorides: determination from first-principles, J. Fluor. Chem. 130 (1) (2009) 38–44.
[25] C. Cazorla, D. Errandonea, High-pressure, high-temperature phase diagram of calcium fluoride from classical atomistic simulations, J. Phys. Chem. C 117 (21) (2013) 11292–11301.
[26] N.T. Wilson, et al., Interionic interactions and fast-ion conduction in CaF_2, J. Chem. Phys. 105 (24) (1996) 11209–11219.
[27] G.D. Barrera, et al., Ionic solids at elevated temperatures and high pressures: MgF2, J. Chem. Phys. 107 (11) (1997) 4337–4344.
[28] H. Kim, Lattice dynamics of magnesium fluoride from a semiempirical two-body potential model, Met. Mater. Int. 7 (1) (2001) 33–37.
[29] M. Liu, et al., Mapping relationships between cation-F bonds and the heat capacity, thermal conductivity, viscosity of molten NaF-BeF2, J. Mol. Liq. 354 (2022) 118915.
[30] J. Morris, et al., Molecular dynamics investigation of threshold displacement energies in CaF2, Comput. Mater. Sci 172 (2020) 109293.
[31] H. Luo, et al., Molecular dynamics simulation of diffusion and viscosity of liquid lithium fluoride, Comput. Mater. Sci 111 (2016) 203–208.
[32] S. He, et al., Molecular dynamics simulation of the structure and properties of CaO-SiO2-CaF2 slag systems, Metall. Mater. Trans. B 50 (3) (2019) 1503–1513.
[33] Z. Zhao-Yi, et al., Phase transition and melting curves of calcium fluoride via molecular dynamics simulations, Chin. Phys. Lett. 25 (1) (2008) 230–233.
[34] H. Guo, et al., First-principles molecular dynamics investigation on KF-NaF-AlF3 molten salt system, Chem. Phys. Lett. 730 (2019) 587–593.
[35] X. Lv, et al., First-principles molecular dynamics study of ionic structure and transport properties of LiF-NaF-AlF3 molten salt, Chem. Phys. Lett. 706 (2018) 237–242.
[36] X. Lv, et al., Molecular dynamics investigation on structural and transport properties of Na3AlF6–Al2O3 molten salt, J. Mol. Liq. 221 (2016) 26–32.
[37] H. Guo, et al., Study on micro-structure and transport properties of KF-NaF-AlF3-Al2O3 system by first-principles molecular dynamics simulation, J. Fluor. Chem. 235 (2020) 109546.
[38] Y. Hu, et al., Electrochemical Behavior of Silicon (IV) Ion in BaF_2 -CaF_2 -SiO_2 Melts at 1573K, J. Electrochem. Soc. 160 (3) (2013) D81–D84.
[39] T. Villalón Jr, Zero-Direct Emission Silicon Production via Solid Oxide Membrane Electrolysis. 2018, Boston University: Boston, MA, USA. p. 147.
[40] S. Su, U. Pal, X. Guan. Zero-direct-carbon-emission aluminum production by solid oxide membrane-based electrolysis process, in: Advances in Molten Slags, Fluxes, and Salts: Proceedings of the 10th International Conference on Molten Slags, Fluxes and Salts 2016, Springer, 2016.
[41] E.S. Gratz, et al., Mitigating electronic current in molten flux for the magnesium SOM process, Metall. Mater. Trans. B 45 (4) (2014) 1325–1336.
[42] X. Guan, U.B. Pal, A.C. Powell, Energy-efficient and environmentally friendly solid oxide membrane electrolysis process for magnesium oxide reduction: experiment and modeling, Metall. Mater. Trans. E 1 (2) (2014) 132–144.
[43] X. Guan, et al., Clean metals production by solid oxide membrane electrolysis process, J. Sustain. Metall. 2 (2) (2016) 152–166.
[44] R.C.D. Mattei, D. Elwell, R.S. Feigelson, Electrodeposition of silicon at temperatures above its melting point, J. Electrochem. Soc. 128 (8) (1981) 1712.
[45] D. Elwell, G.M. Rao, Electrolytic production of silicon, J. Appl. Electrochem. 18 (1) (1988) 15–22.
[46] A.P. Thompson, et al., LAMMPS - a flexible simulation tool for particle-based materials modeling at the atomic, meso, and continuum scales, Comput. Phys. Commun. 271 (2022).
[47] G. Kresse, J. Furthmüller, Efficient iterative schemes for ab initio total-energy calculations using a plane-wave basis set, Phys. Rev. B 54 (16) (1996) 11169–11186.
[48] G. Kresse, J. Furthmüller, Efficiency of ab-initio total energy calculations for metals and semiconductors using a plane-wave basis set, Comput. Mater. Sci. 6 (1) (1996) 15–50.
[49] G. Kresse, J. Hafner, Ab initio molecular dynamics for liquid metals, Phys. Rev. B 47 (1) (1993) 558–561.
[50] J.P. Perdew, K. Burke, M. Ernzerhof, Generalized gradient approximation made simple, Phys. Rev. Lett. 77 (18) (1996) 3865–3868.
[51] G. Kresse, D. Joubert, From ultrasoft pseudopotentials to the projector augmented-wave method, Phys. Rev. B 59 (3) (1999) 1758.
[52] P.E. Blochl, Projector augmented-wave method, Phys. Rev. B Condens. Matter 50 (24) (1994) 17953–17979.
[53] S. Grimme, et al., A consistent and accurate ab initio parametrization of density functional dispersion correction (DFT-D) for the 94 elements H-Pu, J. Chem. Phys. 132 (15) (2010) 154104.
[54] W.G. Hoover, Canonical dynamics: equilibrium phase-space distributions, Phys. Rev. A 31 (3) (1985) 1695–1697.
[55] L. Martínez, et al., PACKMOL: a package for building initial configurations for molecular dynamics simulations, J. Comput. Chem. 30 (13) (2009) 2157–2164.
[56] F.D. Murnaghan, The compressibility of media under extreme pressures, Proc. Natl. Acad. Sci., 30(9) (1944) 244-247.
[57] R. Chahal, S. Banerjee, S.T. Lam, Short- to intermediate-range structure, transport, and thermophysical properties of LiF–NaF–ZrF4 molten salts, Front. Phys. 10 (2022) 830468.
[58] H. Wang, et al., DeePMD-kit: a deep learning package for many-body potential energy representation and molecular dynamics, Comput. Phys. Commun. 228 (2018) 178–184.
[59] L. Zhang, et al., End-to-end Symmetry Preserving Inter-atomic Potential Energy Model for Finite and Extended Systems, 2018.
[60] W. Shinoda, M. Shiga, M. Mikami, Rapid estimation of elastic constants by molecular dynamics simulation under constant stress, Phys. Rev. B 69 (13) (2004).
[61] G.J. Martyna, D.J. Tobias, M.L. Klein, Constant pressure molecular dynamics algorithms, J. Chem. Phys. 101 (5) (1994) 4177–4189.
[62] M. Parrinello, A. Rahman, Polymorphic transitions in single crystals: a new molecular dynamics method, J. Appl. Phys. 52 (12) (1981) 7182–7190.
[63] S. Takamoto, et al., Towards universal neural network potential for material discovery applicable to arbitrary combination of 45 elements, Nat. Commun. 13 (1) (2022) 2991.
[64] A. Birri, et al., Application of the Redlich-Kister expansion for estimating the density of molten fluoride psuedo-ternary salt systems of nuclear industry interest, Chem. Eng. Sci. 260 (2022).
[65] W.R. Grimes, Reactor Chemistry Division Annual Progress Report For Period Ending December 31, 1965, Oak Ridge National Laboratory, 1966. ORNL-3913.
[66] A.D. Kirshenbaum, J.A. Cahill, C.S. Stokes, The density of molten metal fluorides in the range of 1600°–2500°K, J. Inorg. Nucl. Chem. 15 (1960) 297–304.
[67] S. Hu, L.D. Jonghe, Pre-eutectic densification in MgF2-CaF2, Ceram. Int. 9 (4) (1983) 123–126.
[68] Q.-J. Li, et al., Development of robust neural-network interatomic potential for molten salt, Cell Rep. Phys. Sci. 2 (3) (2021).
[69] S. Hara, H. Shibaike, K. Ogino, The molar volumes and the surface tensions of melts in the systems CaF2-MF (M: Li, Na) and CaF2-MF2 (M: Mg, Sr, Ba), ISIJ Int. 30 (4) (1990) 298–304.
[70] M. Korenko, et al., Physico – chemical properties of (MgF2 – CaF2 – (LiF))eut – MgO system as a molten electrolyte for Mg electrowinning, J. Mol. Liq. 275 (2019) 535–543.
[71] B.J. Morgan, vasppy (0.6.3.0), Zenodo (2021), https://doi.org/10.5281/zenodo.4460130.
[72] Y. Sasaki, M. Iguchi, The Coordination of F Ions around Mg and Ca Ions in Molten CaO–CaF2–MgO–SiO2 System at 1873K, ISIJ Int. 49 (4) (2009) 602–604.
[73] P. Bordat, F. Müller-Plathe, The shear viscosity of molecular fluids: a calculation by reverse nonequilibrium molecular dynamics, J. Chem. Phys. 116 (8) (2002) 3362–3369.